JACC: CARDIOVASCULAR IMAGING VOL. 2, NO. 2, 2009

ISSN 1936-878X/09/$36.00
PUBLISHED BY ELSEVIER INC. DOI:10.1016/j.jcmg.2008.11.009

Transmural Myocardial Mechanics During Isovolumic Contraction

Hiroshi Ashikaga, MD, PhD,* Tycho I. G. van der Spoel, MD,†
Benjamin A. Coppola, PhD,* Jeffrey H. Omens, PhD*
San Diego, California; and Utrecht, the Netherlands

OBJECTIVES We sought to resolve the 3-dimensional transmural heterogeneity in myocardial mechanics observed during the isovolumic contraction (IC) phase.

BACKGROUND Although myocardial deformation during IC is expected to be little, recent tissue Doppler imaging studies suggest dynamic myocardial motions during this phase with biphasic longitudinal tissue velocities in left ventricular (LV) long-axis views. A unifying understanding of myocardial mechanics that would account for these dynamic aspects of IC is lacking.

METHODS We determined the time course of 3-dimensional finite strains in the anterior LV of 14 adult mongrel dogs in vivo during IC and ejection with biplane cineradiography of implanted transmural markers. Transmural fiber orientations were histologically measured in the heart tissue postmortem. The strain time course was determined in the subepicardial, midwall, and subendocardial layers referenced to the end-diastolic configuration.

RESULTS During IC, there was circumferential stretch in the subepicardial layer, whereas circumferential shortening was observed in the midwall and the subendocardial layer. There was significant longitudinal shortening and wall thickening across the wall. Although longitudinal tissue velocity showed a biphasic profile; tissue deformation in the longitudinal as well as other directions was almost linear during IC. Subendocardial fibers shortened, whereas subepicardial fibers lengthened. During ejection, all strain components showed a significant change over time that was greater in magnitude than that of IC. Significant transmural gradient was observed in all normal strains.

CONCLUSIONS IC is a dynamic phase characterized by deformation in circumferential, longitudinal, and radial directions. Tissue mechanics during IC, including fiber shortening, appear uninterrupted by rapid longitudinal motion created by mitral valve closure. This study is the first to report layer-dependent deformation of circumferential strain, which results from layer-dependent deformation of myofibers during IC. Complex myofiber mechanics provide the mechanism of brief clockwise LV rotation (untwisting) and significant wall thickening during IC within the isovolumic constraint. (J Am Coll Cardiol Img 2009;2:202–11) © 2009 by the American College of Cardiology Foundation

From the *Departments of Medicine and Bioengineering, University of California, San Diego; and the †Division of Heart and Lungs, University Medical Center Utrecht, Utrecht, the Netherlands. Supported by the American Heart Association 0225001Y (to Dr. Ashikaga, Western States Affiliate) and R01-HL32583 (to Dr. Omens).

Manuscript received August 21, 2008; revised manuscript received October 20, 2008, accepted November 11, 2008.

Myofiber contraction during the isovolumic contraction (IC) phase was considered nearly isometric to build up stress against acute left ventricular (LV) pressure increase (1). However, a number of imaging modalities have uncovered previously unrecognized dynamic aspects of IC (2). For example, there are inward and outward motions of the septal and posterior walls during IC, which are correlated with LV ejection fraction (3). There is also a dynamic

See page 212

LV intracavitary flow during IC (4). In addition, tissue Doppler imaging demonstrated that there is even myocardial shortening during IC (5), which in fact was suggested by earlier studies (6–9). A study using sonomicrometry crystals, has revealed simultaneous subendocardial fiber shortening and subepicardial fiber lengthening (10), although other studies report a lack of heterogeneity in myocardial mechanics during IC (11).

These dynamic aspects of IC seem contradictory to the isovolumic constraint; because the ventricular chamber volume remains constant, overall myocardial deformation during this phase is expected to be little. A unifying understanding of myocardial mechanics during IC that would account for these dynamic aspects of IC is lacking.

Myocardial deformation analysis based on myofibers (12) and myolaminar sheet structures (13) may provide an answer to the apparent contradiction. We determined the time course of 3-dimensional (3D) fiber-sheet strains in the LV anterior wall during IC and ejection in normal dog hearts in vivo with biplane cineangiography of implanted transmural markers.

METHODS

All animal studies were performed according to the National Institutes of Health Guide for the Care and Use of Laboratory Animals.

Surgery. We studied adult mongrel dogs (n = 14, 20 to 30 kg) to measure 3D transmural mechanics in the anterior LV in vivo during atrial pacing. With the dogs placed under general anesthesia and the use of median sternotomy, 3 transmural columns of 4 to 6 0.8-mm diameter markers and a 1.7-mm diameter surface marker above each column were placed within the anterior wall between the first (D_1) and the second diagonal branches (D_2) of the left anterior descending coronary artery (Fig. 1) (14). To provide end points for a LV long axis, 2-mm diameter gold beads were sutured to the apical dimple (apex bead) and on the epicardium at the bifurcation of the left anterior descending and left circumflex coronary arteries (base bead). A pair of pacing wires was sutured to the left atrial surface.

Experiment. Left atrial pacing was performed via a square-wave stimulator at a frequency 10% to 20% above baseline heart rate. Each animal was positioned in a biplane radiography system, and synchronous biplane cineradiographic images (125 frames/s) of the bead markers were digitally acquired with mechanical ventilation suspended at end expiration. The LV pressure, central aortic pressure, left atrial pressure, and surface electrocardiogram (ECG) were recorded simultaneously with the cineradiographic images. At the end of the study, the animal was euthanized with pentobarbital sodium and the heart was perfusion-fixed with 2.5% buffered glutaraldehyde at the end-diastolic pressure measured in the study (14,15). Because the heart was fixed at end-diastolic pressure, fiber and sheet orientations in the fixed hearts were assumed to represent the fiber-sheet structure in the end-diastolic reference configuration in vivo (16).

ABBREVIATIONS AND ACRONYMS

EJ = ejection
IC = isovolumic contraction
LV = left ventricular

Histology. To avoid the distortional effects of dehydration and shrinkage associated with embedding, histological measurements were obtained with freshly fixed heart tissue. In the transmural block of tissue within the implanted bead set, the mean fiber and sheet angles were determined at every 1-mm thick section sliced parallel to the epicardial tangent plane from epicardium to endocardium (14).

Data. The digital images from biplane X-ray were corrected for magnification and spherical distortion (14) to reconstruct the 3D coordinates (17) of the bead markers. Three-dimensional coordinates of the bead markers in each frame were averaged to calculate the location and velocity of the myocardium subtended by the bead set. Six independent finite strains were computed in the local cardiac coordinate system (X_1, X_2, X_3) (Fig. 1B) (18): myocardial stretch or shortening along the circumferential (E_{11}), longitudinal (E_{22}), and radial (E_{33}) axes, and the 3 shear strains (E_{12}, E_{13}, and E_{23}) that represent angle changes between pairs of the initially orthogonal coordinate axes. Another 6 independent finite strains were calculated in the fiber-sheet coordinate system (X_f, X_s, X_n), which defines the muscle fiber axis (X_f), the sheet axis (X_s) that lies within the sheet

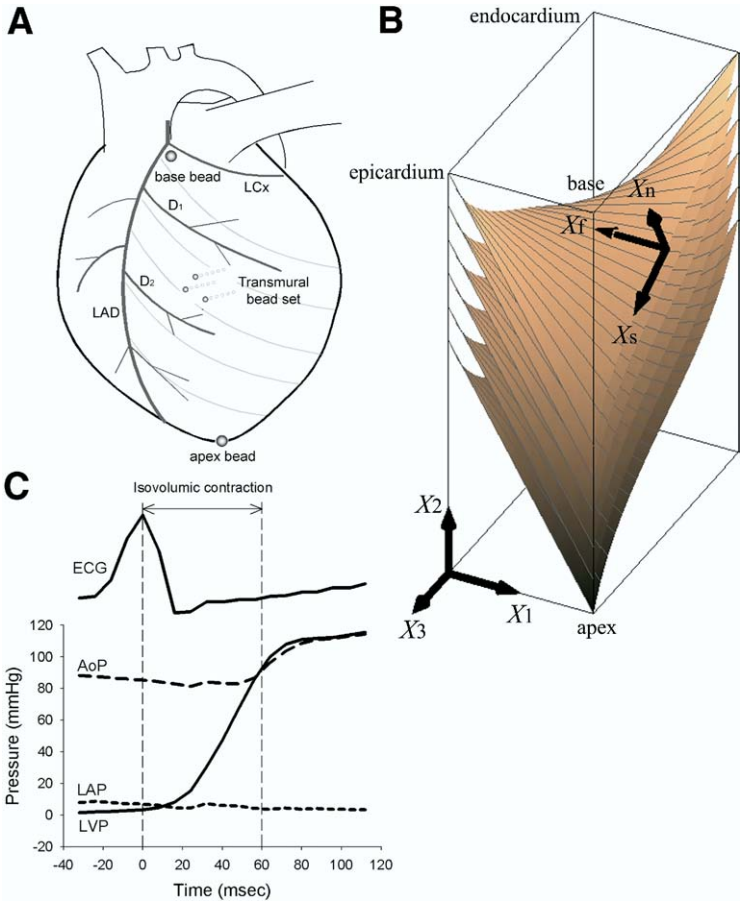

Figure 1. Study Setup

(A) Experimental setup: The transmural bead set (~10 mm) was implanted between the first (D_1) and the second diagonal branch (D_2) of the left anterior descending (LAD) artery. To provide end points for a left ventricular (LV) long axis, gold beads were sutured to the apical dimple (apex bead) and on the epicardium at the bifurcation of LAD and left circumflex (LCx) (base bead). **(B)** LV myocardium within the bead set. The LV myocardium consists of myofibers (X_f) that run parallel to the epicardial tangent plane and are arranged in radially oriented laminae or sheets (X_s). The principal fiber orientation presents a gradual counterclockwise rotation from epicardium to endocardium, resulting in a local architecture of myofibers resembling a spiral staircase with a transmural angle gradient spanning ~120°. The laminar or sheet structure of the myocardium consists of a layered arrangement of myofibers. X_1 = circumferential axis; X_2 = longitudinal axis; X_3 = radial axis; X_f = fiber axis; X_s = sheet axis; X_n = axis oriented normal to the sheet plane. **(C)** Isovolumic contraction (IC) was defined as the period beginning at end diastole (ED) (peak of surface ECG R-wave) and ending at aortic valve opening, which was derived from crossover between LV pressure (LVP) and central aortic pressure (AoP). ECG = electrocardiogram; LAP = left atrial pressure.

plane and is perpendicular to X_f, and the orthogonal X_n axis oriented normal to the sheet plane (19). These strains represent myocardial stretch or shortening along the fiber direction (E_{ff}), the sheet direction (E_{ss}), and normal to the fiber-sheet plane (E_{nn}) and 3 shear strains (E_{fs}, E_{fn}, and E_{sn}) (20). Fiber and sheet angle change from the end-diastolic configuration was calculated at each time frame from deformation data (20).

The data were calculated for each frame (125 frames/s) during contraction as a deformed configuration, with end diastole as the reference state. End diastole was defined at the time of the peak of the ECG R-wave, which is close to the left atrioventricular pressure crossover. The IC phase was defined as the period beginning at end diastole and ending at aortic valve opening, which was derived from crossover between LV pressure and central aortic pressure. The EJ phase was defined as the period beginning at aortic valve opening and ending at aortic valve closure, which was derived from the nadir of the dicrotic notch of the central aortic pressure. The data were determined at 10% increments in time from 0% to 100% during each phase. The strain time course was deter-

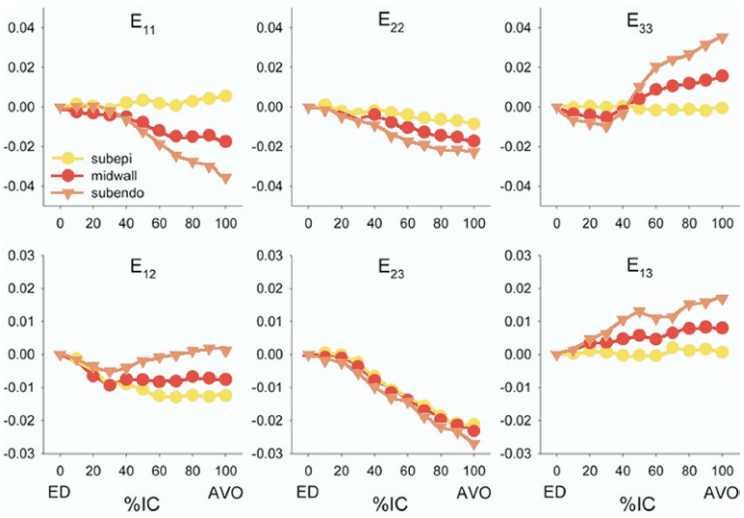

Figure 2. Time Course of Finite Strains in Local Cardiac Coordinates

Values are mean (n = 14). E_{11} = circumferential strain; E_{22} = longitudinal strain; E_{33} = radial strain; E_{12} = circumferential-longitudinal shear strain; E_{23} = longitudinal-radial shear strain; E_{13} = circumferential-radial shear strain. Note different scales for normal and shear strains. AVO = aortic valve opening; ED = end diastole; IC = isovolumic contraction.

mined at three wall depths: 20% (subepicardium), 50% (midwall), and 80% (subendocardium) wall depth from the epicardial surface.

Statistics. Values are means ± SD unless otherwise specified. The effects of wall depth and time on each strain component were determined by 2-factor repeated-measures analysis of variance. The Student-Newman-Keuls method was used for analysis of variance post-hoc analysis. Statistical tests were performed with SigmaStat 3.0 (SPSS Inc., Chicago, Illinois). Statistical significance was accepted at $p < 0.05$.

RESULTS

The site of strain measurement was located at 68 ± 9% of the distance from base to apex along the LV long axis in a region of the anterior LV free wall 1 to 2 cm septal of the anterolateral papillary muscle. Heart rate was 115 ± 22 beats/min, LV end-diastolic pressure was 9.6 ± 4.7 mm Hg, and peak LV pressure was 108.3 ± 17.1 mm Hg. The duration of IC was 59 ± 16 ms.

Local cardiac mechanics. During IC, there was significant longitudinal shortening in all layers (E_{22}, $p = 0.001$) with a significant transmural gradient ($p = 0.013$) (Fig. 2, Table 1). Small circumferential stretch was observed in the subepicardial layer, whereas there was circumferential shortening in the midwall and the subendocardial layer (E_{11}, $p < 0.001$). There was a significant wall thickening (E_{33}, $p < 0.001$), but transmural gradient was not significant ($p = 0.288$). Compared with longitudinal strain, longitudinal location and velocity showed relatively complex changes (Fig. 3). The myocardium moved toward the apex (= positive direction), resulting in a monophasic motion. The myocardial velocity initially increased, then decreased and finally increased again, resulting in a biphasic waveform. During EJ, all strain components showed a significant change over time ($p < 0.001$), which was greater in magnitude than that of IC (Table 1).

Fiber-sheet mechanics. During IC, although the fiber strain did not change significantly overall (E_{ff}, $p = 0.197$), layer-dependent motion in fiber deformation was observed. The subendocardial fibers shortened, whereas the subepicardial fibers lengthened (E_{ff}, Fig. 4), and the transmural gradient was significant ($p < 0.001$). In addition, significant sheet extension (E_{ss}, $p < 0.001$) was observed, thinning (E_{nn}, $p < 0.001$) and fiber-normal shear (E_{fn}, $p = 0.002$) were observed. Fiber-sheet shear (E_{fs}, $p = 0.06$) and sheet shear (E_{sn}, $p = 1.00$) did not show a significant change over time or significant transmural gradient. Fiber angles increased in the subepicardial and midwall and decreased in the subendocardial layer (Fig. 5). Fiber angle change was significant over time ($p = 0.04$) (Table 1). Sheet angles decreased at each depth, resulting in consistently negative sheet angle changes. Sheet

Table 1. Strain Values at AVO and AVC

Strain	Layer	AVO	AVC
E_{11}	Subepi	0.006 ± 0.026*†	−0.069 ± 0.043*†
	Midwall	−0.017 ± 0.033	−0.124 ± 0.056
	Subendo	−0.035 ± 0.037	−0.173 ± 0.059
E_{22}	Subepi	−0.008 ± 0.020*†	−0.038 ± 0.023*†
	Midwall	−0.017 ± 0.033	−0.063 ± 0.032
	Subendo	−0.023 ± 0.038	−0.089 ± 0.034
E_{33}	Subepi	−0.001 ± 0.022*	0.097 ± 0.061*†
	Midwall	0.016 ± 0.036	0.202 ± 0.058
	Subendo	0.035 ± 0.063	0.327 ± 0.097
E_{12}	Subepi	−0.012 ± 0.010*†	0.023 ± 0.024*
	Midwall	−0.008 ± 0.011	0.021 ± 0.020
	Subendo	0.001 ± 0.014	0.010 ± 0.016
E_{23}	Subepi	−0.021 ± 0.017*	0.020 ± 0.038*
	Midwall	−0.023 ± 0.012	0.043 ± 0.028
	Subendo	−0.027 ± 0.024	0.063 ± 0.062
E_{13}	Subepi	0.001 ± 0.019†	0.043 ± 0.032*
	Midwall	0.008 ± 0.017	0.053 ± 0.041
	Subendo	0.017 ± 0.030	0.064 ± 0.076
E_{ff}	Subepi	0.011 ± 0.022†	−0.082 ± 0.042*†
	Midwall	−0.017 ± 0.034	−0.110 ± 0.045
	Subendo	−0.021 ± 0.032	−0.105 ± 0.044
E_{ss}	Subepi	0.016 ± 0.012*	0.031 ± 0.032*†
	Midwall	0.028 ± 0.021	0.101 ± 0.063
	Subendo	0.046 ± 0.054	0.199 ± 0.166
E_{nn}	Subepi	−0.030 ± 0.022*	0.048 ± 0.051*†
	Midwall	−0.025 ± 0.017	0.009 ± 0.097
	Subendo	−0.043 ± 0.028	−0.029 ± 0.151
E_{fs}	Subepi	0.006 ± 0.016	0.033 ± 0.032*
	Midwall	0.006 ± 0.009	0.026 ± 0.026
	Subendo	0.007 ± 0.019	0.073 ± 0.052
E_{sn}	Subepi	0.008 ± 0.024	−0.056 ± 0.038*
	Midwall	−0.008 ± 0.038	−0.099 ± 0.056
	Subendo	0.004 ± 0.054	−0.090 ± 0.178
E_{fn}	Subepi	−0.007 ± 0.012*	−0.017 ± 0.025*
	Midwall	−0.008 ± 0.010	−0.061 ± 0.042
	Subendo	0.001 ± 0.010	−0.057 ± 0.065
Fiber angle change	Subepi	1.4 ± 2.7*	0.1 ± 6.1
	Midwall	0.3 ± 0.7	1.0 ± 1.4
	Subendo	−0.2 ± 1.1	0.9 ± 3.0
Sheet angle change	Subepi	−1.8 ± 2.2*†	4.5 ± 3.4*
	Midwall	−0.9 ± 2.4	7.6 ± 2.8
	Subendo	−2.4 ± 3.0	2.1 ± 11.0
Relative volume	Subepi	0.993 ± 0.028*†	0.959 ± 0.028*†
	Midwall	0.975 ± 0.028	0.941 ± 0.028
	Subendo	0.965 ± 0.045	0.907 ± 0.045

Values are means ± SD. Significant effects ($p < 0.05$) of time (*) and wall depth (†) by 2-way repeated measures analysis of variance during isovolumic contraction and ejection phases are shown in aortic valve opening (AVO) and aortic valve closure (AVC) columns, respectively.

angle changes were significant over time ($p < 0.001$), and there was a significant transmural gradient ($p = 0.045$). Relative myocardial volume underwent significant decrease over time during IC ($p < 0.001$) (Fig. 5, Table 1), and there was a significant transmural gradient ($p = 0.047$). Figure 6 visually illustrates the changes of the normal strain components during IC.

During EJ, all strain components showed a significant change over time (Table 1). Significant transmural gradient was observed in all normal strains (E_{ff}, E_{ss}, and E_{nn}) but not in shear strains (E_{fs}, E_{sn}, and E_{fn}). Although there was no significant fiber angle change over time, sheet angles significantly increased ($p < 0.001$). There was no transmural gradient in either fiber or sheet angle changes.

DISCUSSION

The LV mechanics during IC. Local cardiac mechanics during IC (Fig. 2) are in agreement with previous data in the literature. Radial thickening was recognized in early studies by the use of intramyocardially implanted markers (8,9,21), and longitudinal shortening was reported recently by Edvardsen et al. (5) using tissue Doppler imaging. However, to our knowledge, this is the first study to report layer-dependent deformation of circumferential strain, which results from layer-dependent deformation of myofibers during IC.

Clinically, IC is characterized by a distinct profile of biphasic longitudinal tissue velocity in LV long-axis views by tissue Doppler echocardiography (22). However, the mechanism of the biphasic velocity spikes has not been precisely determined. A recent study by Remme et al. (11) supports the concept that the biphasic velocity spikes reflect early systolic shortening interrupted by mitral valve closure, rather than regional heterogeneity of ventricular contraction (23). Although mitral valve closure certainly plays a role, our data clearly show that tissue deformation in the longitudinal (Fig. 3) as well as other directions (Figs. 2 and 4) is almost linear during IC. This makes a physiologically important point that tissue mechanics during IC, including fiber shortening, is uninterrupted by rapid longitudinal motion created by mitral valve closure. Furthermore, although Remme et al. (11) report lack of heterogeneity in myocardial mechanics during IC, they did not study the transmural heterogeneity of mechanics. Our data clearly demonstrate the presence of transmural heterogeneity of mechanics, which is supported by previous data from Sengupta et al. (10) and our group (24).

We observed subendocardial fiber shortening and subepicardial fiber stretch during IC (Fig. 4, Table 1).

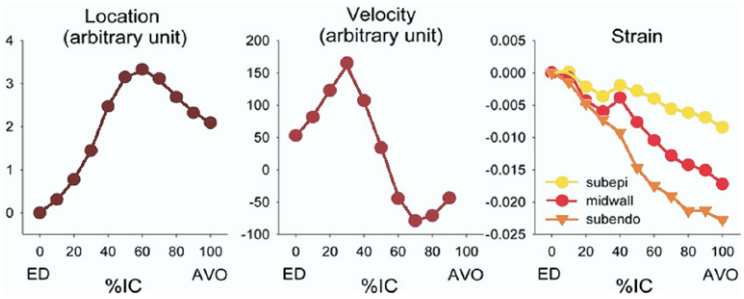

Figure 3. Time Course of Myocardial Location, Velocity, and Strain in the Longitudinal Direction

Values are mean (n = 14). During IC, the myocardium moves toward the apex (=positive direction), resulting in a monophasic motion. The myocardial velocity initially increases, then decreases and finally increases again, resulting in a biphasic waveform. In contrast to the complex change in location and velocity, longitudinal strain shows a relatively straight change during IC. Longitudinal location and velocity are expressed in arbitrary units. Abbreviations as in Figure 2.

This layer-dependent fiber mechanics is consistent with a recent report (10) and provides the mechanism of brief clockwise LV rotation (untwisting) during IC (25–27). Spirally aligned myofibers in the heart convert 1-dimensional fiber deformation into global LV torsional deformation (Fig. 7) (28). IC is a brief period in which endocardial fibers are the predominant source of rotating force because the epicardial fibers are not yet activated. This brief untwisting of the LV does not seem to change the direction of blood flow within the chamber because blood flows from apex to base throughout IC and EJ (4). This layer-dependent counteractive fiber mechanics during IC is also consistent with a hypothesis that the whole ventricular myocardium is one contiguous muscle band ("myocardial band hypothesis"), which has important surgical implications (29). However, as described in our previous report (24), this hypothesis is not supported by anatomical data (12,14).

Fiber angles have traditionally been considered to remain unchanged during the cardiac cycle (12). Our data indicate that the concept is true for EJ, which comprises the vast majority of systole (Table 1). However, our data clearly demonstrate that fiber angles undergo significant change during IC (Fig. 5, Table 1), which has not been documented previously. The angle change was positive and much greater in the subepicardial layer than other layers (Fig. 5). Because subepicardial fiber angles are negative (−20 to ~−30°), a positive angle change indicates that subepicardial fibers become significantly less oblique during IC. This is mechanically consistent with lon-

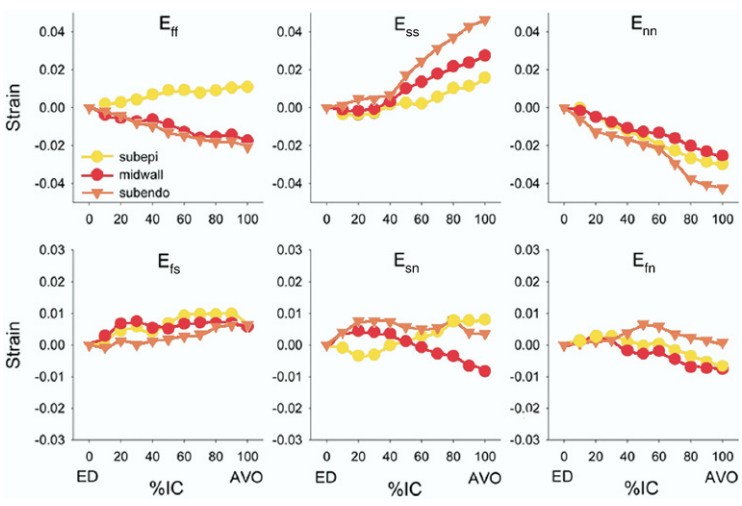

Figure 4. Time Course of Finite Strains in Fiber-Sheet Coordinates

Values are mean (n = 14). Note different scales for normal and shear strains. E_{ff} = fiber strain; E_{ss} = sheet strain, E_{nn} = strain normal to the sheet plane; E_{fs} = fiber-sheet shear strain; E_{sn} = sheet shear strain; E_{fn} = fiber-normal shear strain. Abbreviations as in Figure 2.

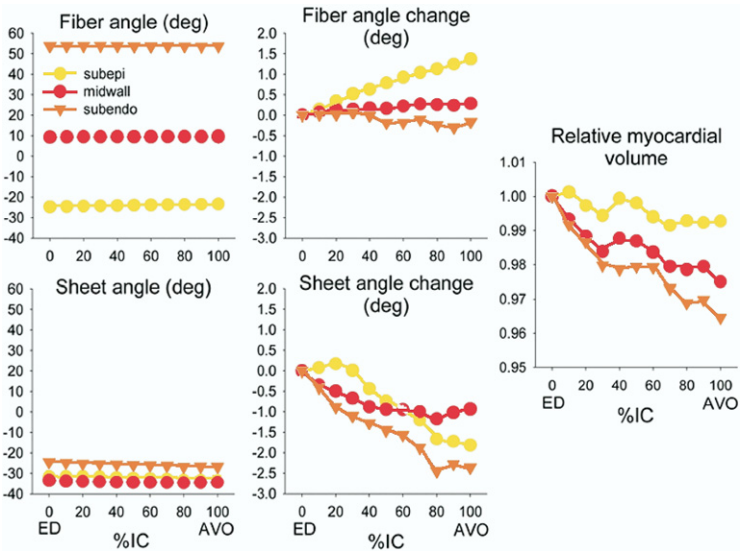

Figure 5. Time Course of Fiber and Sheet Angle Change From the End-Diastolic Configuration and Relative Myocardial Volume

Angles are given in degrees (deg), and the myocardial volumes are expressed as volume relative to 1.00 at end diastole. Abbreviations as in Figure 2.

gitudinal shortening, circumferential stretch, and fiber stretch in the subepicardial layer (Fig. 6) and likely results from tethering by subendocardial fiber shortening during IC.

Normal systolic wall thickening of the myocardium results both from sheet extension and positive sheet angle changes (16). During IC, transmurally uniform sheet extension appears to provide an anatomical basis for radial wall thickening (Fig. 4). In contrast to sheet extension, we found that sheet angle changes were consistently negative over time (Fig. 5, Table 1), which would decrease wall thickness during IC (Fig. 8). This negative sheet angle change counteracts sheet extension to limit wall thickening within the isovolumic constraint.

Clinical implications. This study provides a unifying understanding of myocardial mechanics at the level

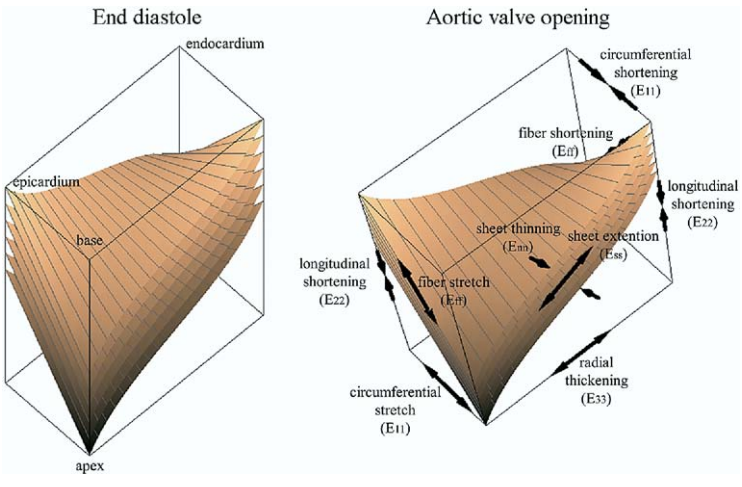

Figure 6. Myocardial Deformation During IC

Significant sheet extension (E_{ss}) and thinning (E_{nn}) occur, which contributes to radial wall thickening (E_{33}). Myofibers shorten (E_{ff}) at the endocardium, which is reflected by circumferential (E_{11}) and longitudinal shortening (E_{22}). In contrast, myofibers stretch (E_{ff}) at the epicardium, which contributes to circumferential stretch (E_{11}) but the myocardium shortens longitudinally (E_{22}). Abbreviations as in Figure 2.

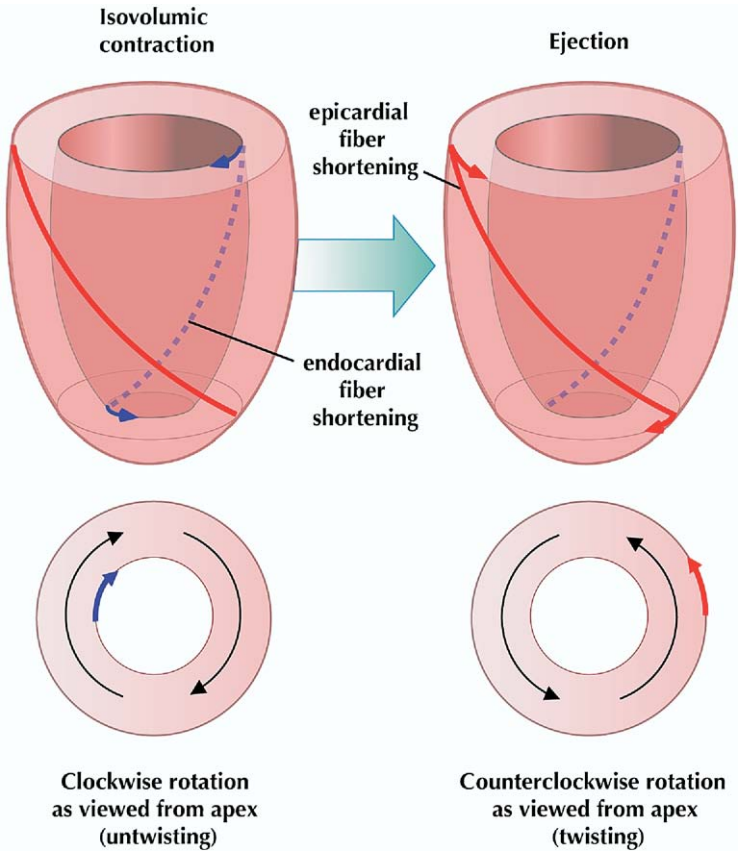

Figure 7. Mechanism of Brief LV Untwisting During IC

During isovolumic contraction, electrical activation initiated in the endocardial Purkinje fibers shortens endocardial fibers **(dashed lines)** wrapped in a right-handed helix. Circumferential components of force **(arrows)** are generated by endocardial fiber shortening, which rotates the LV about the long axis clockwise as viewed from the apex (untwisting). During ejection, electrical activation reaches the epicardium and shortens epicardial fibers **(solid lines)** wrapped in an opposite, left-handed helix, which rotates the LV counterclockwise (twisting). Twisting force by epicardial shortening overcomes untwisting force by endocardial shortening because the torque of the epicardial force is larger because of a greater radius of the epicardial fiber from the central LV long axis. Figure illustration by Rob Flewell. Modified from Ingels et al. (28). LV = left ventricular; other abbreviations as in Figure 2.

cardiac microstructure that accounts for dynamic findings of clinical imaging techniques. Understanding of the physiology during IC combined with noninvasive imaging techniques, including cardiac magnetic resonance, tissue Doppler, and speckle-tracking echocardiography, would help refine therapeutic approaches to heart failure, particularly cardiac resynchronization therapy.

Clinicians need to derive fiber mechanics from variables that are clinically measurable, such as longitudinal, circumferential, and radial strains. If one ignores imbrication angle, a small angle between the epicardial tangent plane and the fiber direction, fiber mechanics can be projected to mechanics in both the longitudinal and circumferential directions. With knowledge of local fiber orientation, fiber mechanics can be reconstructed as weighed sum of longitudinal and circumferential mechanics. For example, Bogaert and Rademakers (30) have calculated fiber mechanics in humans by empirically applying canine fiber orientation data to human mechanics data obtained by clinical cardiac magnetic resonance, assuming that interspecies variation in fiber orientation is negligible (31).

CONCLUSIONS

IC is a dynamic phase characterized by deformation in circumferential, longitudinal, and radial directions which result from complex fiber-sheet motions within the myocardium. Subendocardial fiber shortening provides the mechanism of brief clockwise LV rotation (untwisting), and sheet extension provides anatomical basis for wall thickening. Two counteractive

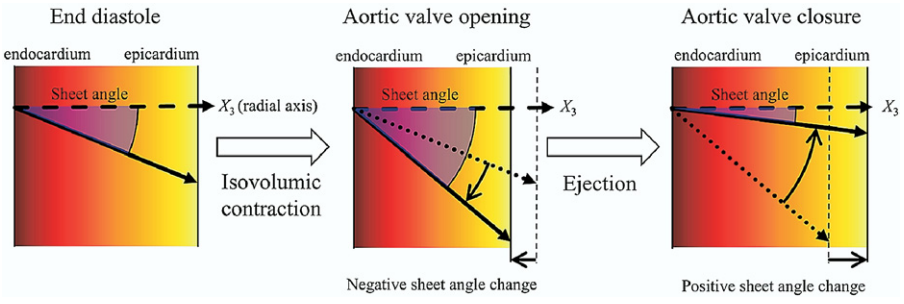

Figure 8. Sheet Angle Change During Isovolumic Contraction and Ejection

Sheet angles are measured with reference to the positive radial axis (X_3). The **left panel** shows a negative sheet angle at end diastole. During isovolumic contraction, there is a significant negative sheet angle change that would act to decrease wall thickness **(center panel)**. During ejection, in contrast, there is a greater positive sheet angle change **(right panel)** that overcompensates the negative sheet angle change during IC, which acts to thicken the wall at aortic valve closure.

motions, sheet extension and negative sheet angle changes, seem to allow significant wall thickening during IC within the isovolumic constraint.

Acknowledgments

The authors thank James W. Covell, MD, for valuable comments and suggestions. The authors thank Rish Pavelec, Rachel Alexander, and Katrina G. Yamazaki for superb managerial and surgical assistance.

Reprint requests and correspondence: Dr. Hiroshi Ashikaga, Division of Cardiology, Johns Hopkins University School of Medicine, 600 North Wolfe Street, Carnegie 568, Baltimore, Maryland 21205. *E-mail: ha8000@gmail.com.*

REFERENCES

1. Wiggers CJ. Studies on the consecutive phases of the cardiac cycle. 1. The duration of the consecutive phases of the cardiac cycle and the criteria for their precise determination. Am J Physiol 1921;56:415–38.
2. Veyrat C, Larrazet F, Pellerin D. Renewed interest in preejectional isovolumic phase: new applications of tissue Doppler indexes: implications to ventricular dyssynchrony. Am J Cardiol 2005;96:1022–30.
3. Pellerin D, Cohen L, Larrazet F, Pajany F, Witchitz S, Veyrat C. Preejectional left ventricular wall motion in normal subjects using Doppler tissue imaging and correlation with ejection fraction. Am J Cardiol 1997;80:601–7.
4. Sengupta PP, Khandheria BK, Korinek J, et al. Left ventricular isovolumic flow sequence during sinus and paced rhythms: new insights from use of high-resolution Doppler and ultrasonic digital particle imaging velocimetry. J Am Coll Cardiol 2007;49:899–908.
5. Edvardsen T, Urheim S, Skulstad H, Steine K, Ihlen H, Smiseth OA. Quantification of left ventricular systolic function by tissue Doppler echocardiography: added value of measuring pre- and postejection velocities in ischemic myocardium. Circulation 2002;105:2071–7.
6. Karliner JS, Bouchard RJ, Gault JH. Dimensional changes of the human left ventricle prior to aortic valve opening. A cineangiographic study in patients with and without left heart disease. Circulation 1971;44:312–22.
7. Bishop VS, Horwitz LD, Stone HL, Stegall HF, Engelken EJ. Left ventricular internal diameter and cardiac function in conscious dogs. J Appl Physiol 1969;27:619–23.
8. Rankin JS, McHale PA, Arentzen CE, Ling D, Greenfield JC Jr., Anderson RW. The three-dimensional dynamic geometry of the left ventricle in the conscious dog. Circ Res 1976;39:304–13.
9. Goetz WA, Lansac E, Lim HS, Weber PA, Duran CM. Left ventricular endocardial longitudinal and transverse changes during isovolumic contraction and relaxation: a challenge. Am J Physiol Heart Circ Physiol 2005;289:H196–201.
10. Sengupta PP, Khandheria BK, Korinek J, Wang J, Belohlavek M. Biphasic tissue Doppler waveforms during isovolumic phases are associated with asynchronous deformation of subendocardial and subepicardial layers. J Appl Physiol 2005;99:1104–11.
11. Remme EW, Lyseggen E, Helle-Valle T, et al. Mechanisms of preejection and postejection velocity spikes in left ventricular myocardium: interaction between wall deformation and valve events. Circulation 2008;118:373–80.
12. Streeter DD Jr., Spotnitz HM, Patel DP, Ross J Jr., Sonnenblick EH. Fiber orientation in the canine left ventricle during diastole and systole. Circ Res 1969;24:339–47.
13. LeGrice IJ, Smaill BH, Chai LZ, Edgar SG, Gavin JB, Hunter PJ. Laminar structure of the heart: ventricular myocyte arrangement and connective tissue architecture in the dog. Am J Physiol 1995;269:H571–82.
14. Ashikaga H, Criscione JC, Omens JH, Covell JW, Ingels NB Jr. Transmural left ventricular mechanics underlying torsional recoil during relaxation. Am J Physiol Heart Circ Physiol 2004;286:H640–7.
15. Yoran C, Covell JW, Ross J Jr. Rapid fixation of the left ventricle: continuous angiographic and dynamic recordings. J Appl Physiol 1973;35:155–7.

16. Costa KD, Takayama Y, McCulloch AD, Covell JW. Laminar fiber architecture and three-dimensional systolic mechanics in canine ventricular myocardium. Am J Physiol 1999;276: H595–607.
17. MacKay SA, Potel MJ, Rubin JM. Graphics methods for tracking three-dimensional heart wall motion. Comput Biomed Res 1982;15:455–73.
18. Meier GD, Ziskin MC, Santamore WP, Bove AA. Kinematics of the beating heart. IEEE Trans Biomed Eng 1980;27:319–29.
19. Costa KD, May-Newman K, Farr D, O'Dell WG, McCulloch AD, Omens JH. Three-dimensional residual strain in midanterior canine left ventricle. Am J Physiol 1997;273:H1968–76.
20. Takayama Y, Costa KD, Covell JW. Contribution of laminar myofiber architecture to load-dependent changes in mechanics of LV myocardium. Am J Physiol Heart Circ Physiol 2002;282:H1510–20.
21. Waldman LK, Nosan D, Villarreal F, Covell JW. Relation between transmural deformation and local myofiber direction in canine left ventricle. Circ Res 1988;63:550–62.
22. Lind B, Nowak J, Cain P, Quintana M, Brodin LA. Left ventricular isovolumic velocity and duration variables calculated from colour-coded myocardial velocity images in normal individuals. Eur J Echocardiogr 2004; 5:284–93.
23. Garcia MJ, Rodriguez L, Ares M, et al. Myocardial wall velocity assessment by pulsed Doppler tissue imaging: characteristic findings in normal subjects. Am Heart J 1996;132: 648–56.
24. Ashikaga H, Coppola BA, Hopenfeld B, Leifer ES, McVeigh ER, Omens JH. Transmural dispersion of myofiber mechanics: implications for electrical heterogeneity in vivo. J Am Coll Cardiol 2007;49:909–16.
25. Yeo SY, Zhong L, Su Y, Tan RS, Ghista DN. Analysis of left ventricular surface deformation during isovolumic contraction. Conf Proc IEEE Eng Med Biol Soc 2007;2007: 787–90.
26. Gibbons Kroeker CA, Ter Keurs HE, Knudtson ML, Tyberg JV, Beyar R. An optical device to measure the dynamics of apex rotation of the left ventricle. Am J Physiol 1993;265: H1444–9.
27. Sengupta PP, Tajik JA, Chandrasekaran K, Khandheria BK. Twist mechanics of the left ventricle: principles and application. J Am Coll Cardiol Img 2008;1:366–76.
28. Ingels NB Jr., Hansen DE, Daughters GT 2nd, Stinson EB, Alderman EL, Miller DC. Relation between longitudinal, circumferential, and oblique shortening and torsional deformation in the left ventricle of the transplanted human heart. Circ Res 1989;64: 915–27.
29. Buckberg GD, Schelbert H, Mahajan A. Cardiac motion and fiber shortening: the whole and its parts. Eur J Cardiothorac Surg 2006;29 Suppl 1:S145–9.
30. Bogaert J, Rademakers FE. Regional nonuniformity of normal adult human left ventricle. Am J Physiol Heart Circ Physiol 2001;280:H610–20.
31. Streeter DD. Gross morphology and fiber geometry of the heart. In: Berne RM, Sperelakis N, editors. Handbook of Physiology. The Cardiovascular System. The Heart. Bethesda, MD: Am Physiol Soc, 1979:61–112.

Key Words: isovolumic contraction ■ cardiac mechanics ■ twisting ■ myofiber ■ sheet.